







Sequential removal of cation/H⁺ exchangers reveals their additive role in elemental distribution, calcium depletion and anoxia tolerance

Iny Elizebeth Mathew¹ | Hormat Shadgou Rhein¹ | Jian Yang¹ |
 Antonella Gradogna²  | Armando Carpaneto^{2,3}  | Qi Guo⁴  | Ryan Tappero⁵ |
 Joachim Scholz-Starke²  | Bronwyn J. Barkla⁴  | Kendal D. Hirschi¹  |
 Tracy Punshon⁶

¹Pediatrics-Nutrition, Children's Nutrition Research, Baylor College of Medicine, Houston, Texas, USA

²Institute of Biophysics, Consiglio Nazionale delle Ricerche, Genova, Italy

³Department of Earth, Environment and Life Sciences (DISTAV), University of Genoa, Genova, Italy

⁴Faculty of Science and Engineering, Southern Cross University, Lismore, New South Wales, Australia

⁵Brookhaven National Laboratory, Photon Sciences Department, Upton, New York, USA

⁶Department of Biological Sciences, Dartmouth College, Hanover, New Hampshire, USA

Correspondence

Kendal D. Hirschi, Pediatrics-Nutrition, Children's Nutrition Research, Baylor College of Medicine, Houston, TX 77030, USA.
 Email: kendalh@bcm.edu

Funding information

National Institutes of Health, Grant/Award Number: R03 AI149201-02; USDA, Grant/Award Number: 3092-51000-061-00D; National Science Foundation, Grant/Award Number: 1557890

Abstract

Multiple *Arabidopsis* H⁺/Cation exchangers (CAXs) participate in high-capacity transport into the vacuole. Previous studies have analysed single and double mutants that marginally reduced transport; however, assessing phenotypes caused by transport loss has proven enigmatic. Here, we generated quadruple mutants (*cax1-4*: qKO) that exhibited growth inhibition, an 85% reduction in tonoplast-localised H⁺/Ca transport, and enhanced tolerance to anoxic conditions compared to CAX1 mutants. Leveraging inductively coupled plasma mass spectrometry (ICP-MS) and synchrotron X-ray fluorescence (SXRF), we demonstrate CAX transporters work together to regulate leaf elemental content: ICP-MS analysis showed that the elemental concentrations in leaves strongly correlated with the number of CAX mutations; SXRF imaging showed changes in element partitioning not present in single CAX mutants and qKO had a 40% reduction in calcium (Ca) abundance. Reduced endogenous Ca may promote anoxia tolerance; wild-type plants grown in Ca-limited conditions were anoxia tolerant. Sequential reduction of CAXs increased mRNA expression and protein abundance changes associated with reactive oxygen species and stress signalling pathways. Multiple CAXs participate in postanoxia recovery as their concerted removal heightened changes in postanoxia Ca signalling. This work showcases the integrated and diverse function of H⁺/Cation transporters and demonstrates the ability to improve anoxia tolerance through diminishing endogenous Ca levels.

KEYWORDS

signalling, stress, SXRF, transport, vacuole

1 | INTRODUCTION

Control of calcium (Ca) ion concentrations is critical for plant function; it is a cell wall component, an enzyme cofactor and a second messenger (Hirschi, 2004). Ca homeostasis is dependent on

membrane transporters, including Ca²⁺-permeable channels, ATP-driven Ca pumps and Ca²⁺/cation antiporters (CaCAs). The CaCA superfamily includes ion-coupled transporters like the Na⁺/Ca²⁺ exchanger, Na⁺/Ca²⁺, K⁺ exchanger, cation/Ca²⁺ exchanger and H⁺/cation exchanger (CAX) (Cai & Lytton, 2004; Pittman &

Hirschi, 2016b). Ca pumps and exchangers are located in multiple membrane systems, including the endoplasmic reticulum (ER), tonoplast and plasma membrane (PM) (Demidchik et al., 2018). Both Ca pumps and CAXs work as vacuolar Ca^{2+} uptake transporters. Ca pumps are considered low-capacity, high-affinity transport systems, whereas CAXs have high capacity and low affinity (Pittman & Hirschi, 2016a). While both Ca pumps and CAXs remove Ca from the cytoplasm, their contributions to control of the magnitude or duration of different stimulus-specific Ca signals remains enigmatic.

Ca can accumulate to millimolar levels in the vacuole, but levels are maintained in the range of nanomolar to low micromolar in the cytosol (Marty, 1999; Schönknecht, 2013). This steep concentration gradient is established with the help of high-capacity H^+ /Ca exchange and Ca pumping (Sze et al., 2000). The driving force for cation antiport activity is the pH gradient generated by two electrogenic proton pumps located on the membrane, an ATPase and a pyrophosphatase (H^+ -PPase) (Sze et al., 1999). H^+ transport processes are integrated with many cellular functions (Strazzer et al., 2019), such as trafficking and hormone perception (Eisenach et al., 2014; Sze & Chanroj, 2018); these processes involve alterations in Ca levels, and H^+ /Ca exchangers may play an essential role in Ca and pH-related signalling events (Pittman et al., 2005).

Plant H^+ /Cation exchangers have previously been cloned using a yeast complementation approach (Hirschi et al., 1996), but the reliance on yeast assays as a proxy for plant-based studies is a limitation of previous CAX studies (Pittman & Hirschi, 2016a). Both yeast and plant studies suggest that CAXs function in the transport of Ca and numerous other cations (Pittman & Hirschi, 2016a). CAX transporters are found in multiple species (Pittman & Hirschi, 2016a), suggesting a pivotal role. The Arabidopsis genome has six CAX open reading frames, but only CAX1-4 have been extensively studied (Manohar et al., 2011a). CAX2 and CAX4 are expressed at lower levels in plants, and most of the work on CAXs in plants has focused on the more highly expressed CAX1 and CAX3 (Conn et al., 2011).

CAX1 is expressed in aerial tissues and CAX3 primarily in the roots (Hocking et al., 2017). Expression of CAX3 is increased in leaves/shoots during stresses such as wounding. There is evidence that CAX1 and CAX3 may function as heterodimers (Hocking et al., 2017), because they are co-expressed in guard cells where they may function singly or together in intracellular signalling (Hu et al., 2015). During stress responses (e.g., pathogen attack or temperature fluctuations), the absence of CAX1 induces ectopic expression of other CAXs, which may help maintain some cellular secretion of Ca to the apoplast (Cheng et al., 2005). High-resolution elemental imaging via synchrotron X-ray fluorescence (SXRF) has shown that *cax1* alters Ca partitioning within cells, reducing Ca partitioning into organelles and/or increasing Ca in the cytosol and abolishing tissue-level Ca gradients (Punshon et al., 2012). *cax1* also has subtle phenotypes in standard growth conditions (Cheng et al., 2003) and shows increased tolerance to anoxia (Yang et al., 2022), serpentine soils (Bradshaw, 2005), freezing (Catalá et al., 2003) as well as altered metal sensitivity (Baliardini et al., 2015), and pathogen defence responses (Yang et al., 2022).

Meanwhile, mutations in both CAX1 and CAX3 cause a significant reduction in plant stature and fertility while maintaining 50% of the tonoplast H^+ /Ca exchange. There is interplay between CAXs and other transporters: deletions in CAX1 reduce the activities of tonoplast Ca^{2+} / H^+ antiporter, tonoplast V-type H^+ -ATPase and increase the activities of tonoplast Ca^{2+} -ATPase and vacuolar Ca^{2+} / H^+ antiporters like CAX3 and CAX4 (Cheng et al., 2003). Given this regulatory interplay (Cheng et al., 2005), deletions in all functional CAXs (CAX 1 to 4) could clarify the role of H^+ /Cation exchange in plant growth and development. Using a battery of phenotyping, omics and elemental imaging techniques, we investigated how the loss of four CAXs impacts growth, membrane transport, elemental distribution and signalling. These findings establish the ability to significantly reduce tonoplast H^+ /Ca exchange and the utility of reducing leaf Ca content by sequentially removing CAXs.

2 | MATERIALS AND METHODS

2.1 | Plant materials and growth

Arabidopsis wild type (Col-0) and CAX mutant seeds (*cax1-1*, *cax3-1*, *cax1-1/cax3-1* double mutant, *cax1-1/cax2-2* double mutant, and *cax1-1/cax4-1* double mutant, *cax1-1/cax3-1/cax4-1* triple mutant and *cax1-1/cax2-2/cax3-1/cax4-1* quadruple mutants) were used in the study. All these mutants were genotyped to confirm the presence of T-DNA insertions (Supporting Information: Figure 16 and Table 24). The seeds were surface sterilised in 20% bleach and grown on a half-MS medium (Murashige and Skoog; Sigma), or low Ca solution (LCS) (Conn et al., 2011) containing 0.5% sucrose and 0.7% agar with a modest addition of CaCl_2 (low Ca media [LCM]—22 mg/L) and were incubated at 12 h light, 22°C, and 12 h night 20°C. For morphological analysis, plants belonging to two rosette leaf stage (Boyes et al., 2001) were transferred to soil and grown at 12 h light, 22°C, and 12 h night 18°C. For checking the Ca^{2+} ion sensitivity of the various mutants, 5-day old plants (cotyledon stage) were transferred to a half-MS medium supplemented with 25 mM CaCl_2 . Growth characteristics were observed 15 days after their transfer to the altered media.

2.2 | Anoxia experiments

For anoxia experiments, 21 days old plants (9 rosette leaf stage) grown under the above-mentioned conditions were placed in an AnaeroPack system (Mitsubishi Gas Chemical) anaerobic atmosphere generation bags (Sigma) with one CampyGen 3.5 L bag (Thermo Scientific). The surgical tapes around the plates were removed before keeping them in the system. The experiment was performed for 10 h unless mentioned otherwise. Experiments were usually done in the nighttime. After the anoxia treatment, plants were returned back to the growth chamber. Images were taken after 4 days using a Nikon D80 Digital SLR Camera (Nikon Corp.).

2.3 | Chlorophyll fluorescence measurement

Chlorophyll estimation was performed as described previously (Liang et al., 2017). Briefly, 50 mg of tissue from both preanoxia and postanoxia samples were ground in liquid nitrogen and a homogenate was prepared in 80% acetone. After centrifugation, the supernatant was collected, and the pellet was re-extracted with 80% acetone. The extraction process was repeated three times until the pellet became colourless. After pooling, the absorbance of the supernatant was measured at wavelengths 645 and 663 nm with a Cary 50 spectrophotometer. Measurement of chlorophyll a, chlorophyll b and total chlorophyll was estimated using Arnon's equation (Arnon, 1949). Plants belonging to the nine-rosette leaf stage were used for the experiment and the whole rosette was isolated 24 h after anoxia treatment. Each experiment was carried out with three to four replicates, and the whole experiment was replicated four times. Statistical significance was calculated using Student's *t*-test and analysis of variance (ANOVA).

2.4 | Combined patch-clamp and fura-2 fluorescence experiments

The *Arabidopsis* mesophyll protoplast isolation procedures and vacuole release were described elsewhere (Gradogna et al., 2021). Patch-clamp recordings were performed in the whole-vacuole configuration using a List Medical amplifier and Pulse acquisition software (HEKA Electronic). Isolated vacuoles were observed using a 40× oil objective (overall magnification 400×) mounted on an inverted Axiovert microscope (Zeiss). Patch pipettes were pulled from thin-walled borosilicate glass capillaries (Harvard Apparatus) and had final resistances of 2–3 MΩ with standard pipette solution containing (in mM): 100 KCl, 3 MgCl₂, 0.4 EGTA, 20 bis-tris-propane, 230 D-sorbitol, pH 7.0 (with MES) and 500 mOsm, supplemented with 100 μM fura-2 pentapotassium salt. The standard (cytosolic) bath solution contained (in mM): 100 KCl, 3 MgCl₂, 2 EGTA, 5 HEPES, 280 D-sorbitol, pH 7.2 (with KOH) and 515 mOsm. Chemicals were purchased from Merck. The vacuole was held at a membrane voltage of -40 mV and continuously perfused with standard bath solution by a gravity-driven perfusion system coupled to a peristaltic pump (Gilson Inc.). For fura-2 detection, a monochromator (Cairn Research) selected the excitation light generated by a Xenon arc lamp (Photon Technology International), alternately at 340 and 380 nm in 100-ms excitation cycles. Fluorescence emission (*F*₃₄₀ for 340-nm excitation and *F*₃₈₀ for 380-nm excitation) was detected using a 515-nm bandpass emission filter and recorded every 300 ms by a CCD camera (Roper Scientific). Fluorescence signals were detected inside a region of interest (ROI) covering the vacuole. MetaFluor software (Molecular Devices) was used to control the system and to calculate online the *F*₃₄₀/*F*₃₈₀ fluorescence ratio. Background fluorescence, measured in an ROI far from the vacuole, was subtracted off-line. After reaching the whole-vacuole configuration, vacuolar fura-2 loading required between 20 and 40 min. Thereafter, a Ca gradient

between the cytosolic side and the vacuolar lumen was established by replacing the standard bath solution with a solution containing (in mM): 100 KCl, 3 MgCl₂, 5 Hepes, 280 D-sorbitol, pH 7.2 (with KOH) supplemented with 10 or 30 μM CaCl₂. The Ca contamination in the Ca²⁺-free solution was less than 2 μM, as determined by atomic absorption spectroscopy.

Experimental conditions were carefully chosen such to exclude any major contribution to the vacuolar Ca²⁺ signals by two-pore channel 1 (TPC1), a highly abundant, Ca-activated vacuolar cation channel permeable to Ca²⁺ (Gradogna et al., 2009). In a series of control experiments on Col-0 and *tpc1* knock-out plants, currents and fluorescence signals were monitored varying [Ca²⁺] and holding voltages.

For fura-2 calibration, fluorescence signals were determined in a 500-μL droplet of standard pipette solution placed onto the bottom of the recording chamber, supplemented with 5 mM EGTA ('zero Ca' condition) and 20 mM CaCl₂ ('saturated Ca' condition). The vacuolar free Ca concentration was then calculated according to the equation (Grynkiewicz et al., 1985):

$$[\text{Ca}^{2+}] = K_d \left(\frac{R - R_{\min}}{R_{\max} - R} \right) \left(\frac{F_{380, \max}}{F_{380, \min}} \right),$$

where *R* is *F*₃₄₀/*F*₃₈₀, *R*_{min} is *F*₃₄₀/*F*₃₈₀ at zero Ca, *R*_{max} is *F*₃₄₀/*F*₃₈₀ in saturated Ca, *F*_{380,max}/*F*_{380,min} is the ratio between *F*₃₈₀ in zero Ca and *F*₃₈₀ in saturated Ca; *K*_d, the dissociation constant of the dye at room temperature, is 224 nM (Grynkiewicz et al., 1985).

Results are given as mean ± standard error (SE). For statistical analysis and graph preparation, Igor Pro (WaveMetrics Inc.) and Excel software (Microsoft Corp.) were used. Statistical significance was determined using Wilcoxon's Rank test.

2.5 | RNA extraction, transcriptomic analysis and quantitative real-time polymerase chain reaction (RT-qPCR)

Total RNA was isolated from 21 days old plants (9-rosette leaf stage) with TRIzol. Whole rosette (50 mg) was ground in liquid nitrogen and homogenate was prepared in TRIzol. Following centrifugation, the upper aqueous phase containing RNA was separated and precipitated with isopropanol. RNA was treated with DNase to remove any contaminating DNA and the quality was assayed by Bioanalyzer.

For transcriptome analysis, RNA samples were outsourced to BGI Genomics (BGI Americas Corporation). RNA-seq was performed using DNBseq platform using 150 bp pair-end sequencing chemistry. A minimum of three independent replicates were used for each condition analysed. All the samples had a RIN value above 7. On average, sequencing yielded 38 million reads per sample. The raw reads were cleaned by removing the adaptors and low-quality sequences. Trimmed reads were then mapped to the reference genome of *Arabidopsis thaliana* obtained from The Arabidopsis Information Resource (TAIR)(TAIR10_Araport11_

[www//.arabidopsis.org_20190423](http://www.arabidopsis.org_20190423)). On average more than 94% of the reads were mapped to the reference genome using STAR v2.7.6a (Dobin et al., 2013). Assembly of RNA-Seq alignments into transcripts was performed using Stringtie2.1.5 (Pertea et al., 2015). The differential gene expression was analysed using edgeR and limma R libraries. RNA-seq data will be deposited in the SRA database with the accession no (pending).

RT-qPCR was used to validate the RNA-seq data. DNase treated RNA was converted into single-stranded cDNA using oligo dT18 primers (SuperScript™ First-Strand Synthesis System for RT-PCR; Invitrogen). For RT-qPCR, 10 ng of the cDNA was used. The quantification was done with iTAQ SYBR Green Master Mix (Bio-Rad) in Biorad CFX96 Real-Time PCR System (Bio-Rad) with gene-specific primers (Supporting Information: Table 25). The reaction consisted of 95°C for 30 s, 40 cycles each of denaturation at 95°C for 5 s and annealing and extension at 60°C for 30 s followed by the additional cycle of 65°C for 5 s and 95°C for 5 s. The expression was normalised to Arabidopsis UBQ10 and the fold changes were calculated by the $2^{-\Delta\Delta Ct}$ method. Statistical significance was calculated by Student's *t*-test in Excel (Supporting Information: Figure 17).

2.6 | Protein isolation, mass spectrometry and protein identification and quantification

Whole rosettes from six-rosette leaf stage plants were used for protein extraction (Barkla et al., 2009). Three grams of tissue was ground in liquid nitrogen and homogenised in prechilled extraction buffer (100 mM Tris-MES, pH 8.0, 1 mM EGTA, 5 mM dithiothreitol, 4 mM MgSO₄, 5% [w/v] insoluble PVP, and plant protease inhibitor cocktails (Sigma) to the recommended concentration by manufacturer). The total proteins in the supernatant (500 µL) were then precipitated using 200 µL 10X TE, 200 µL of 0.3% sodium deoxycholate, and 200 µL of cold 72% TCA. The protein pellets were washed in 90% methanol at room temperature and subsequently lyophilised. Cellular debris was removed by first filtering through Miracloth (Calbiochem), and clarifying by centrifugation.

Protein identification was carried out at the Institute for Molecular Biosciences proteomics facility at the University of Queensland, Brisbane. Proteins were analysed using an Eksigent, Ekspert nano LC400 uHPLC coupled to a TripleTOF 6600+ System (SCIEX) equipped with a PicoView nanoflow ion source (New Objective). Protein extract (up to 5 µL) was injected into a ChromXP C18-CL column (3 µm, 75 µm × 150 mm) (SCIEX). Peptide elution was carried out running linear gradients of 5%–30% solvent B (0.1% formic acid in acetonitrile) over 120 min at 400 nL/min flow rate, followed by 30%–90% solvent B for 3 min, and 90% solvent B for 17 min and was returned to 5% solvent B for equilibration before the next sample injection. Mobile phase used consisted of solvent A; 0.1% formic acid in water, and solvent B; 0.1% formic acid in acetonitrile. The following conditions were used for the experiment; column temperature was maintained at 45°C, ion spray voltage was

set to 2600 V, declustering potential at 80 V, curtain gas flow 25 psi, nebuliser gas 30 psi and interface heater at 150°C. The mass spectrometer was set to acquire 100 ms of full scan TOF-MS data over the mass range 350–1500 *m/z*, followed by up to 50 ms full scan product ion data in IDA mode over the mass range 100–1500 *m/z*. Ions observed in the TOF-MS scan exceeding a threshold of 100 counts and a charge state of +2 to +5 were set to trigger the acquisition of product ion MS/MS spectra of the resultant 50 most intense ions. Protein Pilot 5.0.2 (SCIEX) was used to search spectra against the UniProt Arabidopsis database (proteins, 12 May 2020) and encode the output mzIdentML file for the downstream analysis. Scaffold 4.8.6 (Proteome Software) was used to validate MS/MS-based protein identifications and quantification. Protein identifications were accepted if they could be established at greater than 99% probability and contained at least two unique peptides. Normalised spectral abundance factor (NSAF) was used for protein quantification (Gulcicek et al., 2005; Searle, 2010).

Proteins identified in at least two out of three biological replicates were considered as present in the corresponding genotypes. To evaluate the significance of comparative quantification by different genotypes, Student's *t*-test was performed on the data, and the differences were assigned to be significant at a *p*-value less than 0.05. Differentially abundant proteins (including exclusively present proteins) were submitted to David Bioinformatics Resources 6.8 for Gene Ontology enrichment analysis (Huang, 2009).

2.7 | Real-time measurements of cytosolic Ca in plant leaves postanoxia

CAXs mutants harbouring GCaMP3 sensor (a GFP-based Ca indicator) were generated by crossing the mutants with Col-0 plants harbouring GCaMP3 sensor. Homozygous lines generated in subsequent generations were confirmed by genotyping. Col-0, *cax1-1*, *cax3-1*, *cax1/3/4* harbouring GCaMP3 sensors were surface sterilised in 20% bleach and grown on half-MS medium (Murashige and Skoog; Sigma), containing 0.5% sucrose and 0.7% agar at 21°C till they reached the five-rosette leaf stage. On the day of the imaging experiment, individual plate was foil covered and transferred to a vacuum sealer bag (Wevac) with 1 CampyGen 3.5 L bag (Thermo Scientific) for 4 h. A folded layer of tissue paper was placed between the bag and the plate to avoid any heat stress. GCaMP3 fluorescence was measured immediately after re-exposing the plates to oxygen with a motorised fluorescence stereo microscope (Zeiss Axio Zoom V16) equipped with a PlanApo Z 1.0× objective lens and a Zeiss AxioCam HRm sCMOS camera. GCaMP3 was excited using a mercury lamp (Zeiss HXP 200c Illuminator), with a 470/40 nm excitation filter, and a 500-nm dichroic mirror. The green fluorescent signal passing through a 535/50 nm emission filter was acquired every 1 s using Zeiss Zen pro imaging software. Fluorescence in the entire first true leaf over time was converted into signal values using ImageJ. A similar-sized background was identified and the mean fluorescence over time was subtracted to obtain the actual leaf fluorescence value.

Experiments were run in duplicate each day and experiments were repeated on different days over the course of multiple months until data from at least five replicates were recorded. Statistical analyses were performed with ANOVA and Tukey's post hoc testing or the Student's *t*-test formula in Microsoft Excel. Significance was set at $p < 0.05$. Data were presented as means \pm SEMs.

2.8 | Inductively coupled plasma mass spectrometry (ICP-MS)

Shoots were acid digested by closed vessel microwave-assisted digestion; 1 mL of HNO₃ and 0.1 mL HCl were added to 25 mg of sample and the digestion temperature ramped to 95°C over 15 min and held for a further 45 min. Following digestion samples were diluted to 10 mL with deionized water. Digested samples were analysed by collision cell ICP-MS (Agilent, 8900) operated in helium gas mode. Quality control included initial and continuing calibration checks, three replicate digestion duplicates, spikes and standard reference materials (SRMs) (NIST 1515), analysis duplicates and analysis spikes. Method detection limits and SRM recoveries (%) are given for all elements in Supporting Information: Table 26.

For statistical analyses, after establishing normality, we conducted one-way ANOVA on nonnormalized metal concentration data, with data below detection limits assigned a missing value. Means comparisons were conducted using Tukey's statistical tests. Statistical analysis was conducted in JMP version 16.0.

2.9 | SXRF elemental imaging

Elemental images of leaves were collected at the 4-BM X-Fluorescence Microprobe (XFM) 3-pole wiggler imaging beamline of the National Synchrotron Light Source-II (NSLS-II). XFM has an energy range of 2.3–23 keV, with a flux of $\sim 2 \times 10^{11}$ photons/s (for the Si(111) monochromator). Energy resolution was $\sim 10^{-4}$ ($\Delta\lambda/\lambda$). Our experiments were conducted at 10 keV (optimised for the analysis of Ca), at 10 μ m resolution (10 μ m beam, 10 μ m step) and 50 ms dwell using polychromatic 'pink-beam' mode for rapid imaging. XFM used a Hitachi Vortex ME4 silicon drift detector.

Plants were maintained on solid media in a Conviron™ growth chamber at 22°C with 16/8-h light/dark cycles until analysis. Leaves were cut from actively growing plants with micro scissors immediately before analysis and adhered to single-sided Kapton metal-free tape stretched across custom 35 mm acrylic stage mounts. A size-matched Col-0 leaf was included in each map of transgenic lines for relative abundance comparison. For faster (exploratory) scanning, half of the leaf was scanned at the mid-vein, and full maps were collected from entire leaves, avoiding the cut-edge of the petiole. Mounting times were less than 5 min. For shorter maps (500 pixels²), scan times were approximately 4 h, and for larger maps scan times were approximately 11 h.

Quantification of normalised fluorescence count data into ppm was conducted using the National Institute of Standards and

Technology (NIST) SRM 1833 and 1832. Neither of these SRMs has a certified value for chorine. Data were visualised and scaled using GSE CARS Map Viewer software, which allows user-defined ROI analysis of elemental maps. This was used to compare elemental abundances of lamina and trichomes between transgenic lines.

2.10 | Accession numbers

Sequence data from this article can be found in the GenBank/EMBL data libraries under accession numbers

3 | RESULTS

3.1 | Arabidopsis lines lacking multiple CAXs impaired growth

CAX1 has been known to regulate intracellular Ca²⁺ levels. Plants deficient in CAX1 exhibit Mn²⁺ and Mg²⁺ stress tolerance, a slightly altered ionome and perturbed hormone sensitivities (Cheng et al., 2003, 2005). Further, *cax1* is anoxia and submergence tolerant (Yang et al., 2022), while none of the other three single CAX mutants showed this phenotype (Yang et al., 2022). To determine if impairing these other CAXs had an additive effect on various phenotypes exhibited by *cax1*, we generated lines lacking multiple CAX transporters.

Plants without both CAX1 and CAX3 (dKO-*cax1/3*) have been previously generated (Cheng et al., 2005) while triple (tKO-*cax1/cax3/cax4*) and quadruple mutants (qKO-*cax1/cax2/cax3/cax4*) were developed in this study. These mutants, like dKO, displayed impaired growth and development as plants matured (Figure 1), although there were no significant differences in their germination. During the first several weeks of growth on normal media, these mutants displayed little growth difference compared to Col-0 and *cax1*. However, transferring seedlings to media supplemented with 25 mM CaCl₂ reduced their growth (Figure 1a). A similar result was obtained when the plants were grown in hydroponic basal nutrient solution containing 1 mM Ca (Figure 1b) (Conn et al., 2011); dKO, tKO and qKO lines grew less than Col-0 and *cax1* (Figure 1b). However, when grown hydroponically in an LCS (0.025 mM Ca), this growth difference was reversed, the dKO, tKO and qKO lines had enhanced growth compared to Col-0 (Supporting Information: Figure 1).

Various developmental defects were also observed when plants were grown on half-MS media (10 days old) and transferred to soil. Again, dKO, tKO and qKO lines grew less and slower than Col-0 and the CAX single mutants. As reported previously for dKO (Cheng et al., 2005), tKO and the qKO plants were bushy due to continued lateral branching and necrotic leaf tips (Figure 1c; Supporting Information: Figure 2A). Further, dKO, tKO and qKO did not produce appreciable amounts of viable siliques/seeds (Supporting Information: Figure 2B). The siliques that did form were small and twisted. However, the dKO, tKO and qKO lines grew well

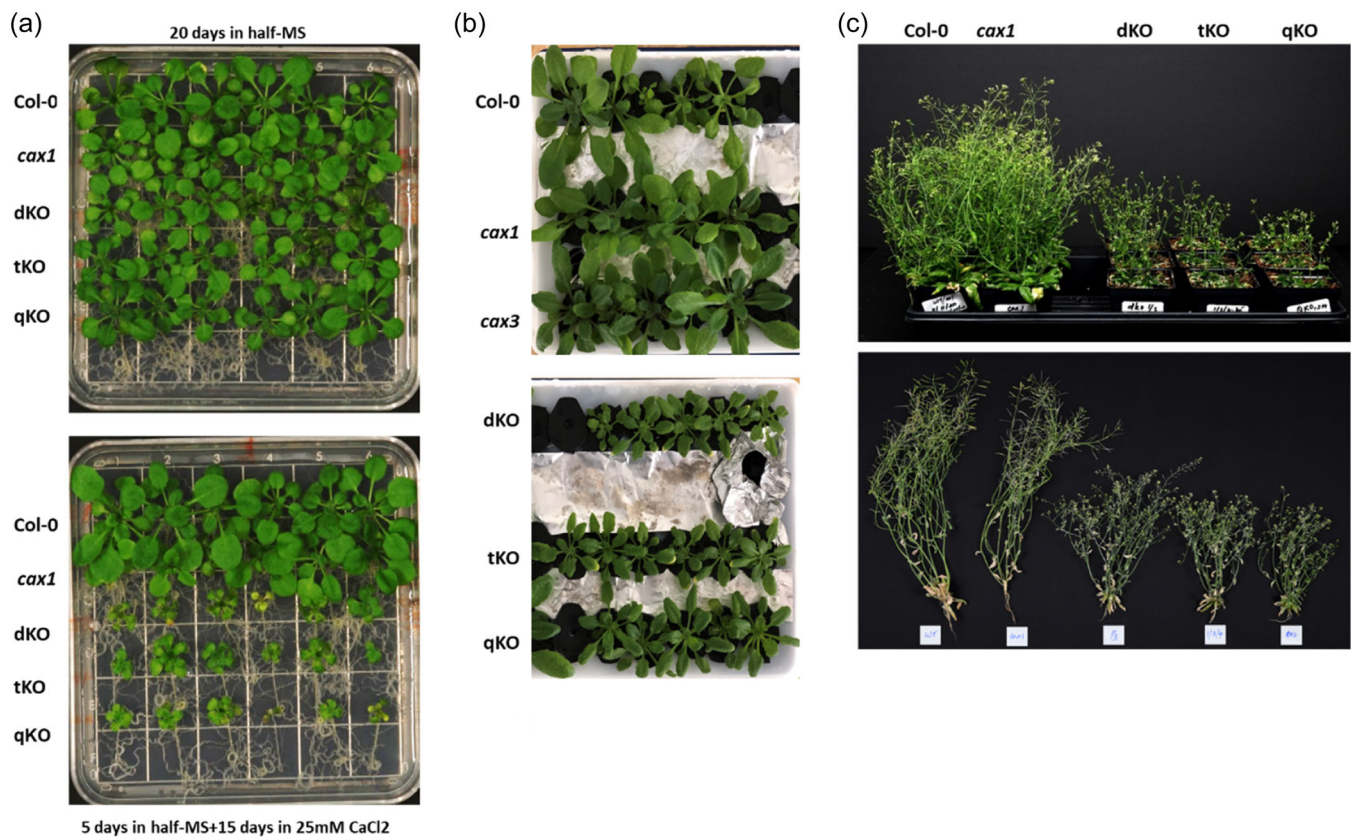


FIGURE 1 Growth characteristics of cation exchangers (CAXs) mutants. (a) Reduced growth of CAX mutants in media containing 25 mM CaCl_2 . Seeds were germinated and grown in a half-MS medium for 15 days before they were transferred to a medium containing calcium (Ca) (lower panel). Photographs were taken 5 days after the transfer to the supplemented medium. Control plants grown on half-MS medium for 20 days are given in the upper panel. (b) Reduced growth of CAX mutants in hydroponic basal nutrient solution containing 1 mM Ca. (c) Altered growth of dKO, tKO and qKO in soil. dKO, tKO and qKOs exhibited much smaller size than Col-0 and *cax1* single mutant. All these plants were grown on half-MS media for 10 days before transferring to the soil.

and produced viable seeds when germinated and grown to maturity in LCS.

3.2 | Vacuoles from qKO plants show severely impaired Ca^{2+} transport

To evaluate the vacuolar Ca uptake capacity of the qKO mutant, we performed combined patch-clamp and microfluometry experiments (Carpaneto et al., 2017; Gradogna et al., 2021) on isolated Arabidopsis mesophyll vacuoles, in which the ratiometric Ca indicator dye fura-2 (Gryniewicz et al., 1985) was loaded into the vacuolar lumen through the patch pipette. After equilibration with the pipette solution, the vacuoles were exposed to bath solutions containing high Ca concentrations $[\text{Ca}^{2+}]$ and the resulting changes in vacuolar fura-2 fluorescence were monitored (Supporting Information: Figure 3). In Col-0 vacuoles, bath application of 10 μM or 30 μM Ca evoked fast and robust increases in the vacuolar $[\text{Ca}^{2+}]$, which were fully reversible upon washout (Figure 2a,c). qKO vacuoles showed strongly diminished vacuolar $[\text{Ca}^{2+}]$ increases at 10 μM Ca (94% reduction compared to Col-0) and attenuated responses at 30 μM Ca in the

bath solution (85% reduction compared to Col-0) (Figure 2b,c). These data suggest that, under our experimental conditions, CAX proteins are largely responsible for Ca uptake capacity in Arabidopsis vacuoles.

3.3 | Altered elemental content in CAX mutants

Bulk elemental composition of Col-0 and CAX mutants leaves under standard growth conditions showed statistically significant differences between Col-0 and CAX mutants Mg, K, Ca, Mn, Fe, Cu and Zn (expressed as mg/kg dry weight; Figure 3a). When lines arranged in order of increasing number of CAX mutations (Col-0, *cax1*, *cax3-1*, dKO, tKO and qKO), the concentration of Mg, K, Ca, Mn, and Zn decreased accordingly whereas Cu showed an increasing trend. Fe concentration in leaves was not influenced by the number of CAX mutations. Leaf Ca concentrations showed the strongest response to CAX mutation ($F = 31.2$, $p < 0.0001$): Ca concentrations in qKO were 58% of Col-0.

The role of CAX transporters in partitioning elements within the leaf has yet to be investigated. We collected elemental data using

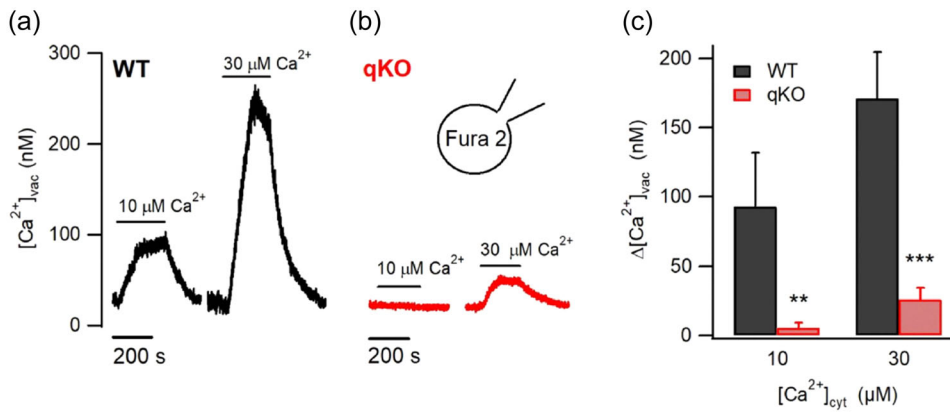


FIGURE 2 Isolated qKO vacuoles show strongly impaired Ca²⁺ accumulation. Fura-2 fluorescence ratio recordings were performed on (a) Col-0 vacuoles and (b) qKO vacuoles, in response to bath application of 10 μM or 30 μM Ca²⁺, as indicated by horizontal bars. Vacuoles were loaded with 100 μM fura-2 through the patch pipette and kept at a membrane voltage of -40 mV. Vacuolar fluorescence ratio values were converted into [Ca²⁺]_{vac} units. (c) Summary plot showing the vacuolar [Ca²⁺]_{vac} changes (Δ[Ca²⁺]_{vac}) evoked by cytosolic Ca²⁺ application at 10 μM (n = 7 vacuoles for both Col-0 and qKO) or 30 μM (n = 14 Col-0 and 18 qKO vacuoles). Data represent mean ± SEM (standard error of the mean). Wilcoxon signed-rank test: **p = 0.0034 for 10 μM Ca²⁺ and ***p = 6 × 10⁻⁶ for 30 μM Ca²⁺.

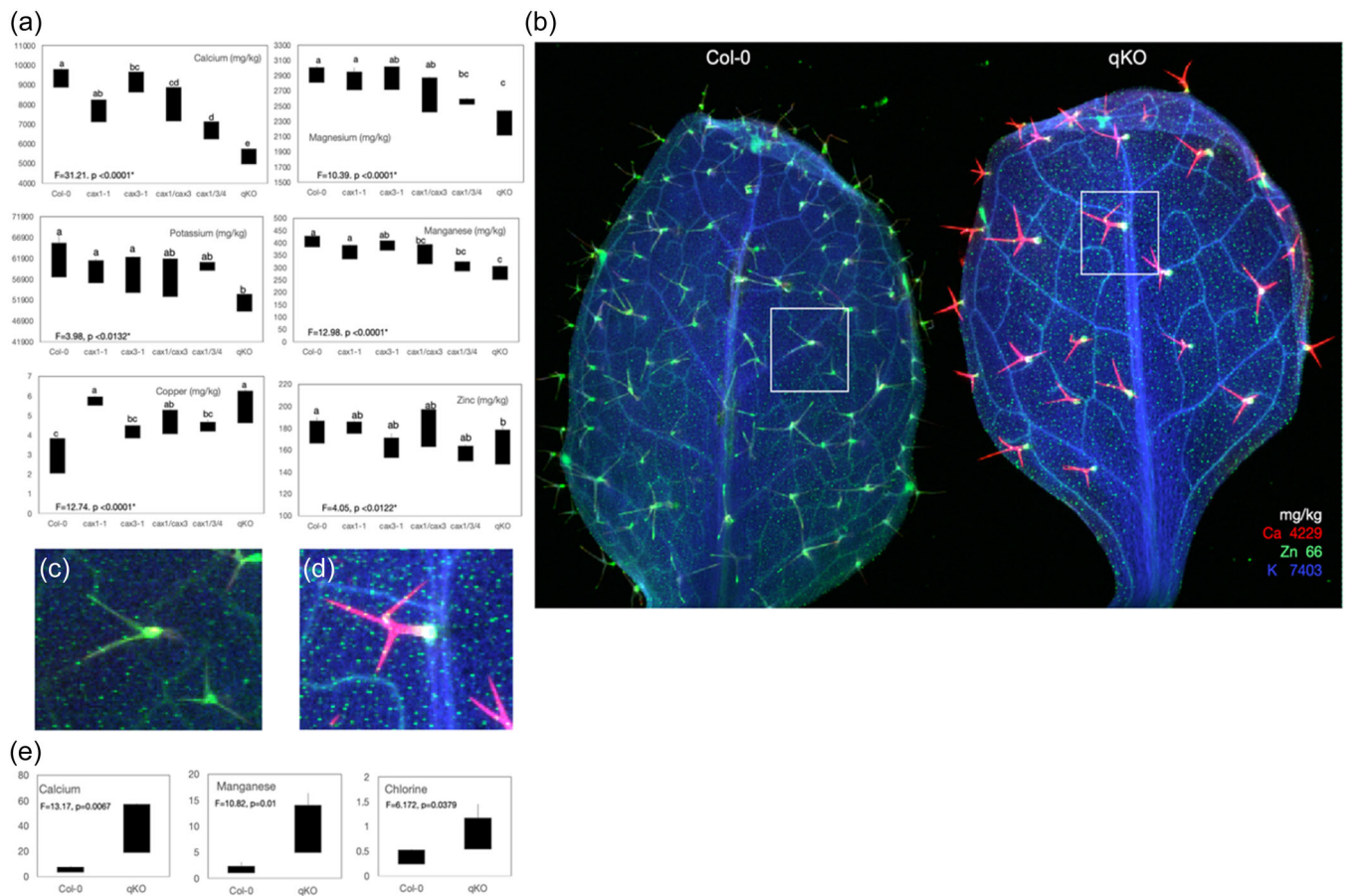


FIGURE 3 Bulk metal concentration and distribution in Col-0 and qKO leaves under normoxic growth conditions. (a) Bulk Ca, Mg, K, Mn, Cu and Zn concentration in shoots (14 days) expressed as mg/kg, with analysis of variance (ANOVA) statistical analysis results indicated with letters denote representing Tukey's means separation. (b) Tricolour synchrotron X-ray fluorescence elemental image of Ca (red), Zn (green) and K (blue) in 14 days old leaves of Col-0 and qKO. Maximum values are shown as mg/kg. (c and d) Zoomed-in images of trichomes (white boxes), showing greater Ca in qKO. (e) User-defined region of interest analysis of trichomes (n = 5, expressed as ion chamber normalised fluorescence counts, averaged to the pixel area) showing results of ANOVA statistical analysis for Ca, Mn and Cl. [Color figure can be viewed at [wileyonlinelibrary.com](https://onlinelibrary.wiley.com/doi/10.1111/pcel.14756)]

two contrasting techniques. Bulk concentration data ($N = 3$) were collected from dried, digested tissue from multiple plants via ICP-MS, and elemental distribution was imaged in fresh, size-matched Col-0 and mutant leaves in the same map ($N = 3$) using synchrotron X-ray fluorescence (SXRF) mapping. Our previous elemental imaging analysis (Punshon et al., 2012) on vacuolar Ca partitioning was conducted on chemically fixed, embedded and sectioned embryonic tissue.

Elemental imaging of the qKO lines allowed us to see how loss of four CAXs impacts mineral distribution and abundance in leaves under normal growth conditions. Elemental images of *cax1* (Supporting Information: Figure 4) agree with the bulk elemental data; changes in Ca in *cax1* are subtle in comparison with qKO. Distributional differences between *cax1* and Col-0 are seen in increased K, higher Ca abundance of the trichomes, and increases in the Zn in the (putative) guard cells. Abundance differences manifest as slightly lower Ca abundances in the vasculature. This is shown alongside the abundance and distributional changes observed in qKO for scale, which were more striking. Elemental images of dKO (Supporting Information: Figure 5), showing partial leaf section from mid-vein to the margin imaged alongside Col-0 in the same map, show greater abundances of Ca in the trichome and more Zn in the stomatal pores in dKO than Col-0.

Elemental images of qKO leaves imaged alongside size-matched Col-0 leaves are shown in Figure 3b. We observed differences in the distribution of K, Ca, Mn, Zn and Cl between Col-0 and QKO. Specifically, we observed more K in vasculature; more Ca, and Mn in trichomes, more Zn in guard cells and more Cl in vasculature. The similarity between dKO and the qKO image is noted in this tricolour image, showing Ca, Zn and K. We observed slightly higher Ca abundances in the trichomes and strikingly higher Zn in putative guard cells in comparison with the co-imaged Col-0 leaf. To explore differences in the trichome further, abundances of elements of Col-0 and qKO trichomes were extracted from elemental images by summing XRF spectra from user-defined regions and generating descriptive statistics from those areas (Figure 3c,d). We chose five trichomes at random from Col-0 and qKO leaf elemental images for comparison and expressed the data on a per pixel-basis, and then conducted ANOVA statistical analysis. This showed that Ca and Mn abundances were significantly higher in qKO than Col-0, and Cl—although not statistically significant—showed the same pattern (Figure 3e).

3.4 | CAX mutants alter the proteome

Proteomic analysis gives insight into the molecular mechanisms responsible for the phenotypic differences observed among Col-0, *cax1* and qKO leaf samples under normoxia conditions. This study identified a total of 1039 proteins from the three genotypes under study with a probability of over 99% with at least two unique peptides (>95% probability) (Figure 4a). Of these proteins, 169, 25 and 58 were detected only in Col-0, only in *cax1*, or only in qKO,

respectively (Figure 4a). Protein abundance was quantified using the NSAF. Principal component analysis (PCA) suggested that there are differences between the proteomes of the mutants compared to Col-0 (Figure 4b). Comparative studies of the protein abundance between the mutants and Col-0 are presented in detail in Supporting Information: Tables 1, 2A and 3.

Compared with Col-0, there are 164 and 70 proteins significantly decreased or increased, respectively, in both *cax1* and qKO. GO enrichment analysis of these proteins highlighted a greater primary metabolic process in Col-0, as showed by the significantly enriched categories including pyruvate metabolic process and starch metabolic process, which was supported by a higher apparent rate of photosynthesis in this line when compared to either *cax1* or qKO (Figure 4c). The observed phenotypes of *cax1* and qKO under normoxia conditions (Figure 1) may be related to suppressed amino acid and fatty acid metabolic processes as highlighted by enrichment of these GO terms in the proteins which increased in abundance (Figure 4b). The mutants also showed enrichment in ribosome biogenesis and response to cold and oxidative stress (Figure 4c). This was supported by the higher abundance of proteins that have oxidoreductase and antioxidant activity (Supporting Information: Table 2B).

The proteomic study also suggested a possible physiological mechanism for the mutant to tolerate abiotic stress. When comparing qKO with Col-0 alone, we found that a large number of proteins involved in chloroplast-localised electron transfer were significantly higher in qKO (AT4G03280, AT4G03280, AT3G15640, ATCG00540, ATCG01060, AT4G23890) (Supporting Information: Table 2A and Figure 6A), even though there was an overall apparent impairment of photosynthetic capacity (PC) in this line. To cope with the large number of electrons leaking from the ETC and generating an excess of reactive oxygen species (ROS), the mutants displayed a stronger sensing and removal system for ROS, such as higher abundance in superoxide dismutase (AT5G18100, AT4G25100), which was also identified as increased in abundance in *cax1* even though not as pronounced as qKO (Supporting Information: Table 3). This was in line with our recent report that the *cax* mutants appear primed for the stress by having heightened expression of ROS-related transcripts (Yang et al., 2022). Furthermore, the oxidative stress induced by ROS may cause the degradation of proteins including those with metal-binding activities (Noctor et al., 2015). This is consistent with a decreased abundance of proteins with metal binding activity (Supporting Information: Table 2 and Figure 6B).

3.5 | Plants lacking multiple cation/H⁺ exchangers have improved anoxia tolerance

Every mutant combination that included *cax1* was tolerant to anoxia (Figure 5; Supporting Information: Figure 7). Tolerance to anoxia increased if an additional CAX gene was impaired. *cax1/2*, *cax1/3* and *cax1/4* lines showed similar anoxia tolerance (Supporting

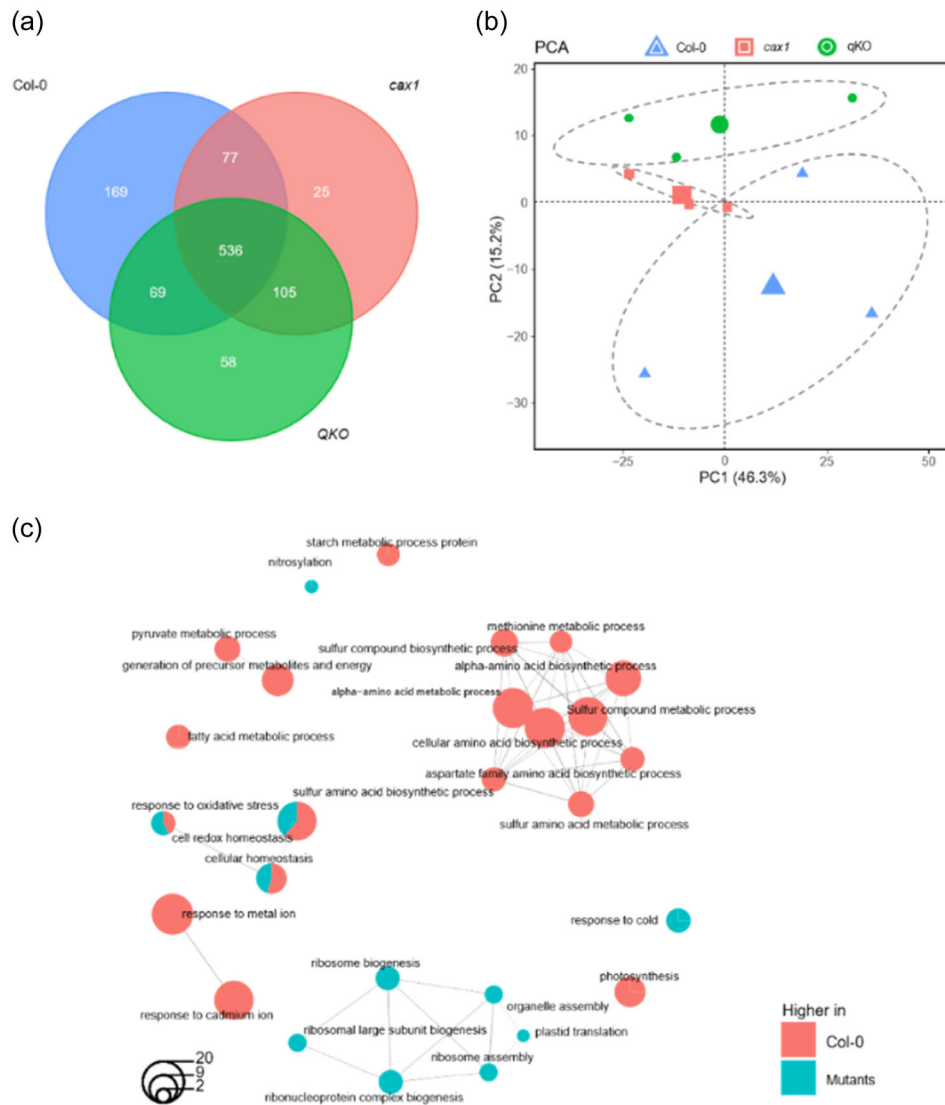


FIGURE 4 Proteomic analysis of Col-0, *cax1* and *qKO* under normoxia condition. (a) Venn diagram showing the overlap between proteins identified in three lines. (b) Principal component analysis (PCA) of the proteome of Col-0, *cax1*, *qKO* under normoxia condition. Sample scores for the first and second principal components were plotted, with the explained percentage of the of PC1 and PC2 indicated along the x and y axes. Clusters corresponding to the groups are represented by 95% confidence ellipses and include data from three biological replicates. The enlarged dots represent the means of the groups. (c) Enrichment network depicting the significantly enriched gene ontology (GO) biological process terms (hypergeometric test with Bonferroni correction, $p < 0.05$) for proteins with higher (blue) or lower (red) abundance in both mutants. Each GO term is represented by a circle, and different groups are shown as different colours. The size of the GO term circle reflects the number of genes/proteins enriched in the corresponding item.

Information: Figure 7A,B). The tKO and qKO lines appeared more tolerant than dKO. The qKO and tKO lines displayed anoxia tolerance even after 20 h of treatment, whereas *cax1* lost its tolerance after 15 h (Figure 5a and Supporting Information: Figure 7C). The response to anoxia, while visually different between tKO and qKO, could not be resolved from chlorophyll measurements following anoxia (Figure 5a,b and Supporting Information: Figure 7B). Further, higher anoxia tolerance of the double, triple and quadruple mutants was linked to their decreased ROS accumulation, confirmed by 3,3'-diaminobenzidine staining (Figure 5c).

3.6 | Plants grown in limiting Ca conditions demonstrate improved anoxia tolerance

cax1/3 mutants (dKO) have improved growth in low-Ca conditions compared to wild-type plants (Conn et al., 2011), and elemental analysis here demonstrates that sequential removal of CAXs reduces Ca content in leaf tissue. We posit that reduced Ca content may be a mechanism by which wild-type plants tolerate anoxia stress and thus sought to grow Col-0 in LCM and assess anoxia tolerance. Unlike Col-0 grown in standard conditions (166 mg/L CaCl₂), Col-0 grown

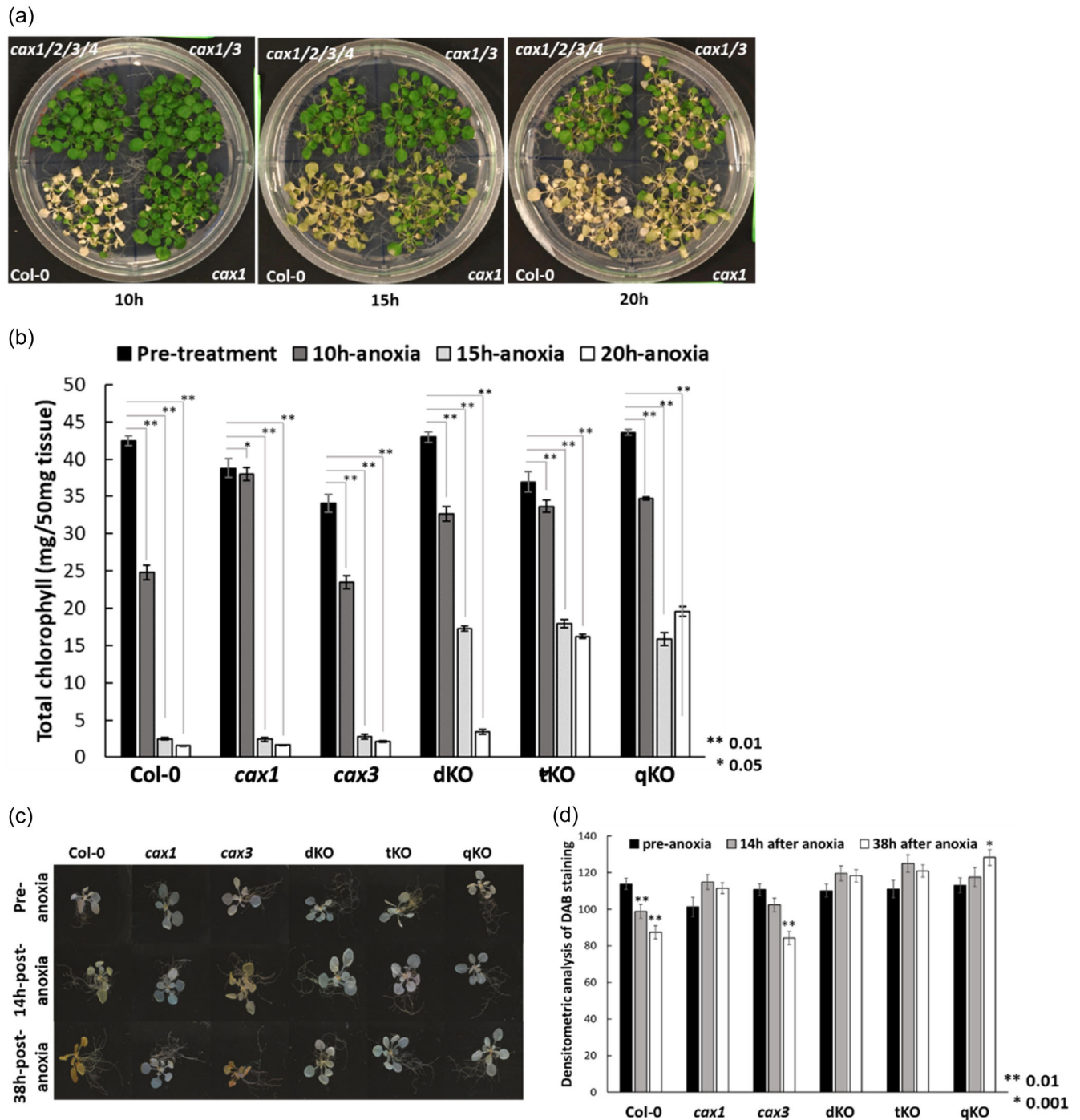


FIGURE 5 Anoxia response of cation exchanger (CAX) mutants. (a) Increased anoxia tolerance of dKO and qKO compared with *cax1* mutant. *cax1* plants lost their tolerance to anoxia after 15 h of treatment, while qKO plants maintained their tolerance even after 20 h of treatment. Twenty-one-day old plants (nine rosette leaf stage) were placed in a GasPack Anaerobic system and were taken out after 10, 15 and 20 h of treatment. These plants were then returned to normoxic conditions and photographed after 5 days. Photographs represent more than three biological replicates. (b) Confirmation of the level of anoxia tolerance in *cax1*, dKO, tKO and qKO by chlorophyll estimation. tKO and qKO plants showed significantly lower chlorophyll loss than dKO after 20 h of anoxia treatment. However, chlorophyll loss was comparable among these genotypes (dKO, tKO and tKO) after 15 h of treatment. *cax1* showed complete loss of chlorophyll after 15 h of treatment. There was no significant difference in the levels of chlorophyll loss between tKO and qKO at any time points analysed. Experiments were performed as mentioned in (a). Data indicated are a representative of three biological replicates and asterisk indicates significant difference from the pretreatment conditions as calculated by ANOVA asterisks (* $p \leq 0.05$ and ** $p \leq 0.01$). Error bars represent standard error from the mean value. (c) Decreased H_2O_2 accumulation in the CAX mutants as indicated by 3,3'-diaminobenzidine (DAB) staining. A dark brown precipitate in Col-0 and *cax3* indicate the presence of H_2O_2 . Whole rosettes from 3-week old plants were exposed to anoxic conditions for 10 h. Rosettes were sampled 14 and 38 h after the plants were brought back to normoxic growth conditions. Unstressed plants (preanoxia) were used as the control. Data shown are a representative of more than three independent experiments. (d) Quantification of DAB staining by software ImageJ. Nine leaves from three different plants were used for quantification. Asterisks indicate significant difference compared to preanoxia condition as calculated using Student's *t*-test in Excel (* $p \leq 0.01$ and ** $p \leq 0.001$).

for 3 weeks in LCM (22 mg/L CaCl₂) displayed anoxia tolerance like the CAX mutants (Figure 6).

3.7 | RNAseq analysis of CAX mutants reveals their additive role in anoxia tolerance

We showed differential gene expression between the anoxia-sensitive (Col-0, *cax3*) and tolerant (*cax1*) lines (Yang et al., 2022).

To determine how CAX transport contributes to tolerance, dKO and qKO were subject to RNAseq. The leaves of 21-day-old plants (nine-rossette leaf stage) were harvested at the start of the treatment (0-h control-pre), after being in the anoxia chamber for 4-h (anoxia) and 1-h post-7-h anoxia treatment (postanoxia). Each library consisted of at least 38 million reads (>94%) mapped to the Col-0 genome. RNAseq analyses were done for Col-0, *cax1* (Yang et al., 2022) and dKO before, during and after anoxia and qKO before and after anoxia (Figure 7). Treatments and mutants clearly clustered separately in

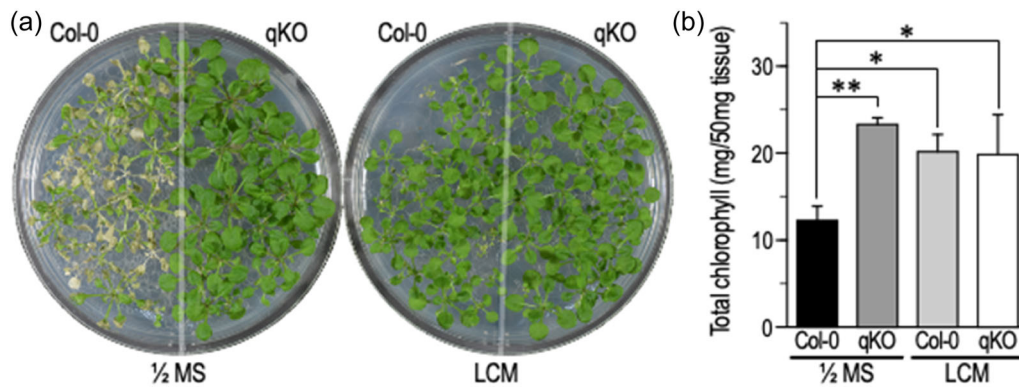


FIGURE 6 Anoxia response of Col-0 grown in low-Ca-containing media (LCM). (a) Increased anoxia tolerance of Col-0 grown in LCM compared to Col-0 grown in 1/2 MS. Twenty-one-day old plants (nine rosette leaf stage) were placed in a GasPack Anaerobic system and were taken out after 8 h of treatment. These plants were then returned to normoxic conditions and photographed after 4 days. Photographs represent more than three biological replicates. (b) Confirmation of anoxia tolerance by chlorophyll estimation. Col-0 in LCM and qKO plants grown in both media conditions showed significantly lower chlorophyll loss than Col-0 growth in 1/2 MS 20 h postanoxia. Experiments were performed as mentioned in (a). Data are representative of three replicates. Asterisks indicate significant differences between the samples as calculated by two-way ANOVA $p < 0.05$ for * and $p < 0.005$ for **. Error bars represent standard deviation from the mean value. [Color figure can be viewed at [wileyonlinelibrary.com](https://onlinelibrary.wiley.com/doi/10.1111/pcel.14756)]

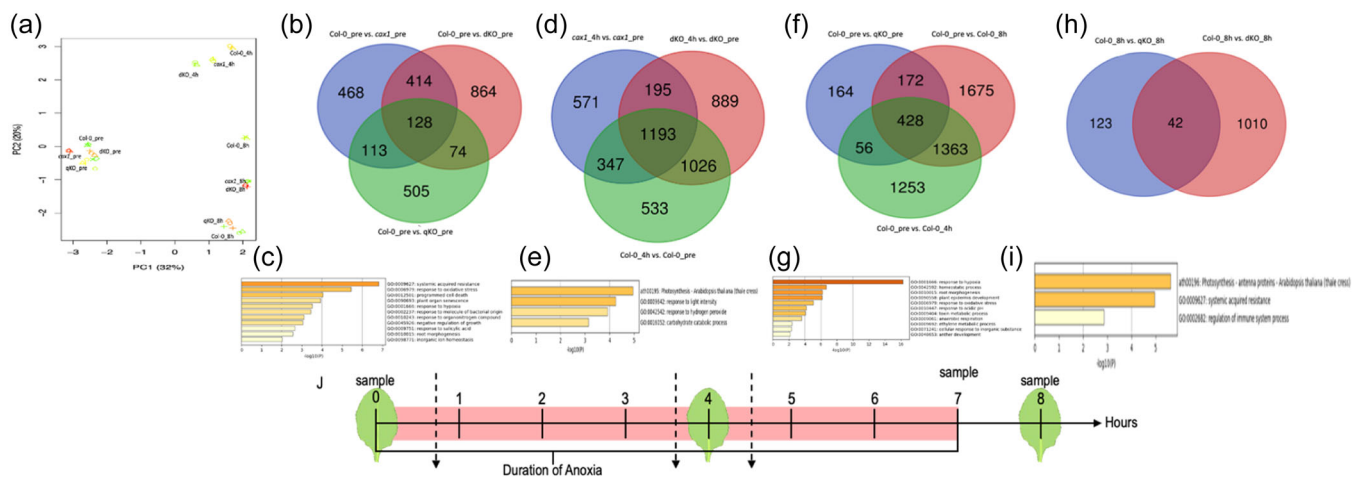


FIGURE 7 Cation exchangers (CAXs) mutants transcriptome-wide responses to anoxia. (a) Principal component analysis (PCA) plot representing the transcriptomes of Col-0, *cax1*, *cax1/3* and *cax1/2/3/4* before, during and after anoxic treatment. (b) Upregulated genes in *cax1*, dKO and qKO compared during normoxia condition. (c) Gene ontology (GO) biological pathway analyses are for the 128 common upregulated genes in all the three mutant lines. (d) Upregulated genes in Col-0, *cax1* and dKO during anoxia. (e) GO biological pathway analyses are for the 195 common upregulated genes in *cax1* and dKO that are not found in Col-0. (f) Upregulated genes in qKO during normoxia and Col-0 during and postanoxia. (g) GO biological pathway analyses are for the 428 common upregulated genes in qKO during normoxia and Col-0 during and postanoxia. (h) Upregulated genes in dKO and qKO compared to Col-0 postanoxia. (i) GO biological pathway analyses are for the 42 common upregulated genes in dKO and qKO. (j) Scheme and timing of leaf tissue harvesting for RNA-seq analysis. Plants belonging to nine rosette leaf stage were taken for RNA-seq analysis before anoxia (preconditions), after 4 h of anoxia (anoxia) and 1 h after a 7-h anoxia treatment (postanoxia).

PCA showing the first and second PCs which together explained 52% of variances, suggesting differences between responses in the various genotypes (Figure 7a).

Similar to our previous analyses (Col-0, *cax3* and *cax1* [Yang et al., 2022]), a large number of genes responded significantly to the treatment during and after anoxia. 3099 genes were upregulated in Col-0 during anoxia while 4879 genes were downregulated (Supporting Information: Tables 4 and 5). The gene ontology (GO) category for upregulated genes included cellular response to oxygen (Supporting Information: Figure 8A) and downregulated genes included those involved in photosynthesis (Supporting Information: Figure 8B). Postanoxia, 3638 genes were upregulated with GO categories for cellular response to hypoxia (Supporting Information: Figure 9A and Table 6) and 2873 genes were downregulated representing GO categories related to photosynthesis (Supporting Information: Figure 9B and Table 7). Having RNA-seq libraries from dKO and qKO allows further inferences to be drawn on the role of cation/H⁺ exchange in anoxia tolerance. We hypothesised that enhanced expression or repression of specific genes before the stress primes *cax1* for anoxia, which confers tolerance (Yang et al., 2022). During normoxia, *cax1* (1123 genes), dKO (1480) and qKO (820) lines had heightened expression of genes related to defence, oxidative stress and programmed cell death (Figure 7b,c, Supporting Information: Tables 8–10). We found that approximately 10% (116/1123) of the genes expressed at higher levels in *cax1* during normoxia were expressed in Col-0 during anoxia (Supporting Information: Figure 10A). This increased in dKO and qKO: approximately 13% (192/1480) in dKO and 40% (320/820) in qKO (Supporting Information: Figure 10A). The same trend was observed with genes highly expressed in mutants during normoxia compared to Col-0 postanoxia (*cax1*: 61/1123–5%; dKO: 308/1480–20%; qKO: 426/820–51%) (Supporting Information: Figure 10C). Enriched GO categories for the upregulated genes in qKO normoxia that were upregulated in Col-0 during anoxia and postanoxia were clearly related to hypoxia (Figure 7f,g, Supporting Information: Table 11). When *cax1* and dKO were included in the analysis, the GO terms were response to oxidative stress, secondary metabolic biosynthesis and defence (Supporting Information: Figure 10E,F and Table 12).

We also analysed the down regulated genes among the CAX mutants in normoxia conditions and few commonly shared down regulated genes were found (Supporting Information: Figure 11A and Table 13). However, many genes downregulated in the mutants during normoxia were downregulated in Col-0 during anoxia (*cax1*: 7/57–12%; dKO: 192/563–34%; qKO 17/48–35%) with a smaller percentage of overlap in downregulated genes with Col-0 postanoxia (*cax1*: 3/57–5%; dKO: 136/563–24%; qKO 6/48–12.5%) (Supporting Information: Figure 12 and Tables 14–16).

During anoxia, compared to Col-0, *cax1-1* (*cax1* throughout the remainder of the manuscript) and dKO both expressed 195 genes that were related to photosynthesis, response to light intensity, hydrogen peroxide and carbohydrate catabolic process (Figure 7d,e,

Supporting Information: Table 17). Additionally, 361 genes related to defence, organ senescence and response to salicylic acid were down regulated in *cax1* and dKO during anoxia (Supporting Information: Figure 11B,C and Table 18). Postanoxia, dKO and qKO both showed unique expression of 42 genes related to photosynthesis and defence that were not expressed in Col-0 (Figure 7h,i, Supporting Information: Table 19). Postanoxia qKO showed downregulation of 525 genes, many of these involved in hypoxia responses and hormone signalling in comparison to Col-0 (Supporting Information: Figure 11D,E and Table 20). A total of 193 genes repressed in both qKO and dKO appeared to be involved in long-chain fatty acid metabolism, response to water, and stomatal function (Supporting Information: Figure 11D,F and Table 21).

We mined the expression data for increased or decreased expression of genes highly responsive to H⁺/Ca, depending on the number of CAX mutants (*cax1* > dKO > qKO and qKO > dKO > *cax1*). From 128 common upregulated genes during normoxia (Figure 7b), 20 fit the expression pattern of *cax1* > dKO > qKO (these genes were related to regulation of development and root morphogenesis) (Supporting Information: Figure 13A,B and Table 22) and 6 had the expression pattern of qKO > dKO > *cax1* (Supporting Information: Figure 13C and Table 23). None of the downregulated genes fit the pattern of *cax1* > dKO > qKO.

3.8 | Both CAX1 and CAX3 participate in Ca signalling postanoxia

Given that CAX1 is highly expressed in leaves, it could be the primary H⁺/Ca exchanger involved in postanoxia Ca signalling in the aerial portion of the plant (Pittman & Hirschi, 2016a). Previous work demonstrates that Ca signals are significantly different between the anoxia-tolerant *cax1* and anoxia-sensitive Col-0 during reoxygenation (Yang et al., 2022); here we aim to identify if CAX3 (dKO vs *cax1*) and CAX4 (dKO vs tKO) also influence leaf Ca signalling postanoxia. Stable transgenic lines of dKO and tKO expressing cytoplasmic GCaMP3 (a GFP-based Ca biosensor; Yang et al., 2022) were used to visualise the progression of Ca signals in the cytoplasm following anoxia and wounding (Supporting Information: Movie 1). The mutants showed no changes during wounding but reoxygenation after exposing the plants to 4 h of anoxia treatment resulted in differences in the temporal signals produced in dKO and tKO, compared to *cax1*. In the older leaves (first pair of true leaves/leaf 1) of dKO and tKO, a strong initial signal peaked at around 100 s (111 and 125 s for dKO and tKO, respectively), compared to the first signal at 201 s in *cax1* (Figure 8a,b, Supporting Information: Figure 14A,B and Movie 1); the dKO and tKO lines are similar, suggesting that CAX4 has a minimal role in this response. However, the response in these mutants is different than *cax1* and Col-0, highlighting the importance of CAX3. In most cases, Ca fluorescence intensity was found to be higher in both dKO and tKO (Supporting Information: Figure 14A). In the younger leaves (leaf 3), the Ca signal peaked at around 100 s and was present in all the mutant genotypes with slight variation in the

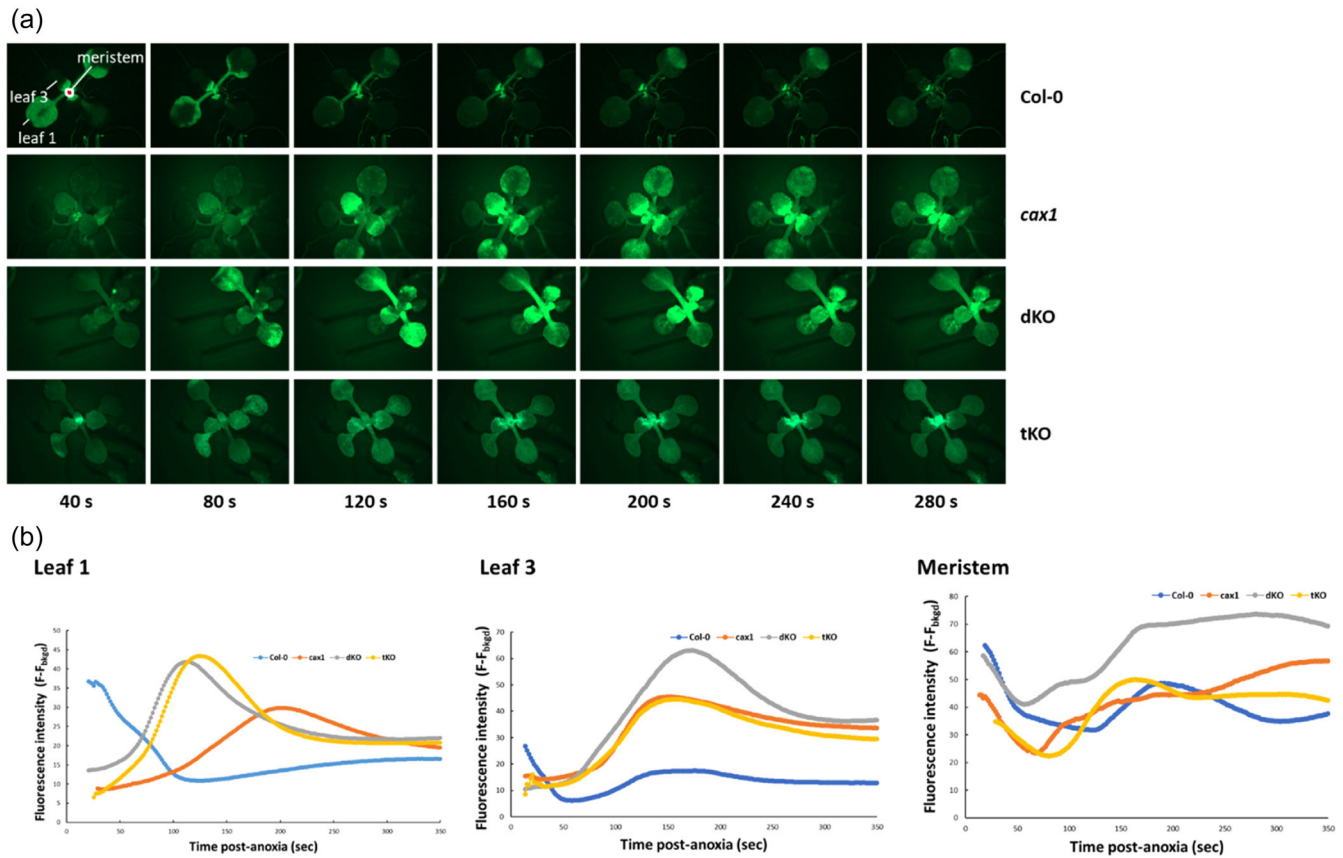


FIGURE 8 Calcium (Ca) changes in Col-0, *cax1*, dKO and tKO during exposure to oxygen after anoxia stress. Col-0, *cax1*, dKO and tKO stably expressing the genetically encoded Ca²⁺ indicator, GCaMP3, were grown on 1/2MS with 0.5% sucrose for 12 days and were treated with anoxia stress for 4 h. The intensity of fluorescence of GCaMP3 was recorded using a fluorescence microscope immediately after the plants were re-exposed to oxygen. (a) Representative images of plants expressing the GCaMP3 Ca²⁺ biosensor at different time points as 40, 80, 120, 160, 200, 240 and 280 s after exposing them to normoxic conditions. (b) Quantification of fluorescence of the selected genotypes during reoxygenation after anoxia stress. The region of interest is outlined as in Figure 8a. Representative of ≥ 3 independent plants/leaves. [Color figure can be viewed at wileyonlinelibrary.com]

intensity (Supporting Information: Figure 14A). This suggests that CAX3 and CAX4 have a limited role in postanoxia Ca signalling in these leaves. As shown previously (Yang et al., 2022), older Col-0 leaves had a prominent initial Ca signal, which dissipated in the first 50 s (Supporting Information: Figure 14A) and a second minor signal after 150/160 s. The pattern was similar in the younger leaves, but with lower fluorescence intensity (Figure 8a,b and Supporting Information: Movie 1). A clear signal was present in the meristematic region in all the genotypes, during the entire imaging interval (6 min). A drop in the intensity was observed at around 100 s in all genotypes (Figure 8a,b, Supporting Information: Movie 1). This suggested that in the meristem, the CAXs have a minor role in shaping the Ca signal postanoxia. In this experiment, plants were imaged immediately after exposing them to normoxia conditions. However, it took ~15–30 s to unseal the anoxic chamber and start imaging. Thus, the data represented lack the information for the initial time frame (15–30 s following reoxygenation). We ensured that the changes in the Ca dynamics in the CAX mutants are specific to anoxia stress by analysing the Ca signals in these genotypes following wounding

(Supporting Information: Figure 15A,B). All four genotypes showed a similar cytoplasmic Ca dynamic. Mostly, the signal was limited to the leaf in which the stress was induced meaning it does not produce Ca changes at a whole plant level (Supporting Information: Figure 15A) and plants showed a gradual increment in the intensity of the Ca signal following wounding, which peaked between 50 and 80 s and then showed a decline (Supporting Information: Figure 15B). Additionally, we did not observe any statistical difference in the Ca signals between Col-0 and *cax* mutants during normoxia conditions (Supporting Information: Figure 15C), further confirming that the sensor is working in the same way in different genotypes.

4 | DISCUSSION

This work characterises plants lacking four functional CAX transporters. This quadruple mutant has pleiotropic phenotypes and offers an unparalleled biological resource to discern the role of high-capacity low-affinity tonoplast localised H⁺/Ca transport in plant signalling

and elemental repartitioning (Figures 3–8). The transport assay is a technical innovation and demonstrated the most significant reduction in plant H^+/Ca transport yet reported (Figure 2). The elemental analysis established how these transporters work together to repartition multiple elements and reduce endogenous Ca levels (Figure 3). Using RNAseq, proteomic and Ca-imaging approaches established that these CAX mutants sequentially alter plants' expression patterns and signalling pathways to promote anoxia tolerance (Figures 4, 5, 7 and 8). These findings led to an original hypothesis that reduced endogenous Ca levels in plants confer anoxia tolerance. This hypothesis was supported by demonstrating that wild-type plants grown in reduced Ca media had anoxia-tolerant phenotypes similar to CAX mutants (Figure 6).

Previous studies have demonstrated different transport properties and tissue localisation of the CAXs (Pittman & Hirschi, 2016a, 2016b); this study continues to clarify the roles of these transporters. CAX1 and CAX3 (dKO) loss also appeared to be a tipping point for changes in Ca signalling and elemental distribution in leaves during normoxia conditions (Figures 3 and 8); meanwhile, previous studies have suggested CAX3 had a minimal role in Ca homeostasis in aerial tissues (Manohar et al., 2011b). Postanoxia Ca signalling in leaves changed more dramatically in the dKO and tKO lines than *cax1*, demonstrating that CAX3 impacts anoxia responses through changes in Ca signalling (Figure 8). In the *cax1* background, each additional CAX mutation lowered Ca levels in the leaf tissue (Figure 3), altered leaf protein and gene expression (Figures 4 and 7) and increased anoxia tolerance (Figures 5 and 6). These phenotypes suggested all four CAXs can function in leaf tissue.

Plant Ca signalling is a complex process with many transporters altering cytosolic Ca levels (Sanders et al., 2002). The reduced tonoplast transport in qKO may increase Ca sequestration into other endomembrane compartments and cause changes in capacitance Ca entry (store-operated entry) (Berridge et al., 2000; Costa et al., 2018; Hogan & Rao, 2015): in qKO lines, ER and other endomembrane Ca stores might communicate a 'filled state' to the PM to diminish endogenous Ca levels (Figure 2) and alter Ca signalling and nutrient sensing (Schachtman and Shin, 2007) (Figure 8). Alterations in CAXs impact proton pumps (Cheng et al., 2003) and future work will need to be directed at determining how the drastic change in tonoplast Ca transport affects the dominant proton pumps such as the PM ATPase, the vacuolar pyrophosphatase (V-PPase), and the vacuolar-type ATPase (V-ATPase).

4.1 | Mutations in CAXs significantly alter mineral partitioning and abundance in leaves

The altered transport in the qKO mutants (Figure 2) impacted changes in elemental abundance and distribution in leaf tissue (Figure 3). These changes were not seen in *cax1* and were not significantly altered by loss of CAX2 and CAX4. The most striking differences were in dKO and qKO were (1) remobilisation of Ca to the trichomes, (2) increased Zn in what we assume are the guard cells

and (3) increased Cl levels throughout the lamina and vasculature (Figure 3; Supporting Information: Figure 4). The characteristic punctate Zn distribution was a consistent observation in our leaf images. Because the CAXs do not appear to transport Zn, these images indicated that abolishing CAX-mediated transport affects Zn distribution. Published whole leaf Zn maps are scarce, but our previous study (Hindt et al., 2017) analysing altered Fe homeostasis displays a similar but less pronounced, punctate Zn phenotype.

Likewise, Cl is not thought to be transported by CAXs, nor has it consistently been measured in studies of the CAXs, but was perturbed in qKO, which had more Cl in the trichomes (Figure 3e). Chlorine may play a pivotal role in osmotic regulation (Colmenero-Flores et al., 2019), and this perturbation could indirectly result from CAX deletion. The SXRF observations indicate a cascade of changes resulting from a change of CAX-mediated transport, underscoring the multielemental interplay when biological systems are perturbed and the advantages of taking a multielemental analytical approach.

Bulk concentrations of Ca in qKO leaves were lower than wild type, *cax1*, dko and tKO, as were Mn, Mg, K, and Zn, although to lesser extents (Figure 3). However, these quantitative changes were less apparent in the elemental imaging. Comparisons between spatially resolved and volume-averaged concentrations could be more intuitive. They should be made cautiously: bulk analysis averages out elemental concentrations across the whole shoot biomass of many plants, whereas elemental images focus on a single leaf at the micron scale, and trends area function of scale. Higher abundances of Ca in the trichome of qKO (Figure 3e) cannot be extrapolated to an increase in Ca abundance of the entire shoot biomass, as much as it indicates a remobilisation of Ca.

In qKO Ca abundance was higher in the trichomes (Figure 3e); a significant storage location for metals in various flowering plant species. Trichomes have long been known as a mineral storage location for plants (Ricachenevsky et al., 2021). Some hyperaccumulator species store potentially toxic, nonessential metals and Ca in trichomes (Broadhurst et al., 2004). Mutants in CAX1 are tolerant to serpentine soils (Bradshaw, 2005) and Cd stress (Baliardini et al., 2015), and the altered metal distribution or elemental abundance documented here may help explain these phenotypes (Whitt et al., 2020).

4.2 | Sequential removal of CAXs reveals their additive role in anoxia responses

The sequential disruption of CAX transporters allowed a more thorough examination of the role of H^+/Ca disruption in anoxia tolerance: anoxia tolerance is not due to the loss of specific transport properties of CAX1. If this were the case, the dKO, tKO and qKO lines would be equally tolerant to anoxia as *cax1*. Anoxia tolerance is probably not caused by changes in apoplastic free Ca levels, because this is a dKO phenotype (and presumably also present in tKO and qKO) not seen in *cax1* (Conn et al., 2011). Furthermore, stomatal movement and phosphate homeostasis are unaffected in *cax1* (Cho et al., 2012;

Liu et al., 2011), suggesting that anoxia tolerance does not result from these changes. A knockout of *CAX1* in *Arabidopsis* alters tolerance to various metals, Ca-depleted conditions, and freezing after cold acclimation (Baliardini et al., 2016; Bradshaw, 2005; Catalá et al., 2003). We posit these phenotypes are caused by altered Ca, or pH homeostasis at the tonoplast (Cheng et al., 2003) and, given the modified transport properties observed here, will be more robust in dKO, tKO and qKO. The *CAX* mutants may have numerous adaptations that allow them to endure anoxia stress (Yang et al., 2022): an essential component of this tolerance could be decreased internal Ca levels and the constitutive expression of a suite of anoxia tolerance genes (Figures 5 and 7). This work demonstrates that during normoxia, qKO had elevated expression of approximately 40% of the genes Col-0 expresses at high levels during or postanoxia. Many of these genes are involved in defence, but some are involved in hypoxia responses (Figure 7f,g, Supporting Information: Table 11). Similar comparisons using dKO, while not as dramatic as those with qKO, further support the idea that *CAX* mutants may be anoxia tolerant due to changes in gene expression present before anoxia stress. In agreement with this, qKO also showed changes to cellular redox homeostasis at the proteomic level, with increased abundance in enzymes involved in ROS production and removal when compared to Col-0 (Supporting Information: Table 2) (Paradiso et al., 2016). The mutants are primed for anoxic conditions, as the proteomic analysis indicates that the absence of *CAXs* already imposed stresses, which was reflected by reduced growth which we posit is caused by changes in carbon fixation and carbohydrate metabolism (Figures 1 and 4). Given that wild-type plants grown in reduced Ca-containing media are anoxia tolerant (Figure 6), it will be interesting to determine if these growing conditions impact the expression of stress genes and elemental partitioning.

5 | CONCLUSIONS

The loss-of-function of *CAXs*—diminishing Cation/H⁺ exchange—appears to have adaptive advantages, with a 'less is more' phenotype regarding Cation/H⁺ exchange activity and anoxia tolerance (Figures 1 and 4) (Yang et al., 2022). Few studies have demonstrated the additive positive effects of multiple loss-of-function transport mutants in plant stress responses. Loss-of-function alleles were once the epitome of deleterious genetic variation (Xu et al., 2020). This study further appreciates the reduction of *CAX* activity as an adaptation to plant stress (Baliardini et al., 2016; Bradshaw, 2005; Catalá et al., 2003; Modareszadeh et al., 2021). It will be interesting to survey various plants to delineate if diminished *CAX* function and changes in Ca content increase stress tolerance (Clemens, 2006; Fones et al., 2019); if such plants exist, how do they compensate for impaired *CAX* function during normal growth conditions?

ACKNOWLEDGEMENTS

We thank Ardawna Green for help growing the plants. Simon Gilroy for help establishing the calcium imaging procedures and Jon Pittman for reading an early version of this work. This research used the

X-Fluorescence Microprobe (XFM) beamline (4-BM) of the National Synchrotron Light Source II, an US Department of Energy (DOE) Office of Science User Facility operated for the DOE Office of Science by Brookhaven National Laboratory under Contract No. DE-SC0012704. This work was supported by grants to Tracy Punshon and Kendal D. Hirschi from the National Science Foundation (1557890), and grants to Kendal D. Hirschi from USDA (3092-51000-061-00D) and National Institute of Health (R03 AI149201-02). This research used beamline 4-BM of the National Synchrotron Light Source, an US Department of Energy (DOE) Office of Science User Facility operated for the DOE Office of Science by Brookhaven National Laboratory under Contract No. DE-AC02-98CH10886. ICP-MS analysis was carried out at the Dartmouth Trace Element Core Facility, which is supported by Dartmouth Cancer Centre with NCI Cancer Centre Support Grant 5P30 CA023108.

ORCID

Antonella Gradogna  <http://orcid.org/0000-0002-4401-9913>

Armando Carpaneto  <http://orcid.org/0000-0002-5060-3657>

Qi Guo  <http://orcid.org/0000-0002-3528-2533>

Joachim Scholz-Starke  <http://orcid.org/0000-0002-7376-6635>

Bronwyn J. Barkla  <http://orcid.org/0000-0002-4691-8023>

Kendal D. Hirschi  <http://orcid.org/0000-0001-6122-3222>

REFERENCES

- Arnon, D.I. (1949) Copper enzymes in isolated chloroplasts. polyphenoloxidase in *Beta Vulgaris*. *Plant Physiology*, 24, 1–15.
- Baliardini, C., Corso, M. & Verbruggen, N. (2016) Transcriptomic analysis supports the role of CATION EXCHANGER 1 in cellular homeostasis and oxidative stress limitation during cadmium stress. *Plant Signaling & Behavior*, 11(6), e1183861.
- Baliardini, C., Meyer, C.L., Salis, P., Saumitou-Laprade, P. & Verbruggen, N. (2015) CATION EXCHANGER1 cosegregates with cadmium tolerance in the metal hyperaccumulator *Arabidopsis halleri* and plays a role in limiting oxidative stress in *Arabidopsis* Spp. *Plant Physiology*, 169, 549–559.
- Barkla, B.J., Vera-Estrella, R., Hernández-Coronado, M. & Pantoja, O. (2009) Quantitative proteomics of the tonoplast reveals a role for glycolytic enzymes in salt tolerance. *The Plant Cell*, 21, 4044–4058.
- Berridge, M.J., Lipp, P. & Bootman, M.D. (2000) The versatility and universality of calcium signalling. *Nature Reviews Molecular Cell Biology*, 1, 11–21.
- Boyes, D.C., Zayed, A.M., Ascenzi, R., McCaskill, A.J., Hoffman, N.E., Davis, K.R. et al. (2001). Growth stage-based phenotypic analysis of *Arabidopsis*: a model for high throughput functional genomics in plants. *Plant Cell*, 13(7), 1499–1510. <https://doi.org/10.1105/tpc.010011>
- Bradshaw Jr, H.D. (2005) Mutations in *CAX1* produce phenotypes characteristic of plants tolerant to serpentine soils. *New Phytologist*, 167, 81–88.
- Broadhurst, C.L., Chaney, R.L., Angle, J.S., Mangel, T.K., Erbe, E.F. & Murphy, C.A. (2004) Simultaneous hyperaccumulation of nickel, manganese, and calcium in *Alyssum* leaf trichomes. *Environmental Science & Technology*, 38, 5797–5802.
- Cai, X. & Lytton, J. (2004) The Cation/Ca²⁺ exchanger superfamily: phylogenetic analysis and structural implications. *Molecular Biology and Evolution*, 21, 1692–1703.
- Carpaneto, A., Boccaccio, A., Lagostena, L., Di Zanni, E. & Scholz-Starke, J. (2017) The signaling lipid phosphatidylinositol-3,5-bisphosphate

- targets plant CLC—a anion/H(+) exchange activity. *EMBO Reports*, 18, 1100–1107.
- Catalá, R., Santos, E., Alonso, J.M., Ecker, J.R., Martínez-Zapater, J.M. & Salinas, J. (2003) Mutations in the $\text{Ca}^{2+}/\text{H}^{+}$ transporter CAX1 increase *CBF/DREB1* expression and the cold-acclimation response in *Arabidopsis*. *The Plant Cell*, 15, 2940–2951.
- Cheng, N.-H., Pittman, J.K., Barkla, B.J., Shigaki, T. & Hirschi, K.D. (2003) The *Arabidopsis* *cax1* mutant exhibits impaired ion homeostasis, development, and hormonal responses and reveals interplay among vacuolar transporters. *The Plant Cell*, 15, 347–364.
- Cheng, N.-H., Pittman, J.K., Shigaki, T., Lachmansingh, J., LeClere, S., Lahner, B. et al. (2005) Functional association of *Arabidopsis* CAX1 and CAX3 is required for normal growth and ion homeostasis. *Plant Physiology*, 138, 2048–2060.
- Cho, D., Villiers, F., Kroniewicz, L., Lee, S., Seo, Y.J., Hirschi, K.D. et al. (2012) Vacuolar CAX1 and CAX3 influence auxin transport in guard cells via regulation of apoplastic pH. *Plant Physiology*, 160, 1293–1302.
- Clemens, S. (2006) Toxic metal accumulation, responses to exposure and mechanisms of tolerance in plants. *Biochimie*, 88, 1707–1719.
- Colmenero-Flores, J.M., Franco-Navarro, J.D., Cubero-Font, P., Peinado-Torruibia, P. & Rosales, M.A. (2019) Chloride as a beneficial macronutrient in higher plants: new roles and regulation. *International Journal of Molecular Sciences*, 20, 4686.
- Conn, S.J., Gilliam, M., Athman, A., Schreiber, A.W., Baumann, U., Moller, I. et al. (2011) Cell-specific vacuolar calcium storage mediated by CAX1 regulates apoplastic calcium concentration, gas exchange, and plant productivity in *Arabidopsis*. *The Plant Cell*, 23, 240–257.
- Costa, A., Navazio, L. & Szabo, I. (2018) The contribution of organelles to plant intracellular calcium signalling. *Journal of Experimental Botany*, 69(17), 4175–4193. <https://doi.org/10.1093/jxb/ery185>
- Demidchik, V., Shabala, S., Isayenkov, S., Cuin, T.A. & Pottosin, I. (2018) Calcium transport across plant membranes: mechanisms and functions. *New Phytologist*, 220, 49–69.
- Dobin, A., Davis, C.A., Schlesinger, F., Drenkow, J., Zaleski, C., Jha, S. et al. (2013) STAR: ultrafast universal RNA-seq aligner. *Bioinformatics*, 29, 15–21.
- Eisenach, C., Baetz, U. & Martinoia, E. (2014) Vacuolar proton pumping: more than the sum of its parts? *Trends in Plant Science*, 19, 344–346.
- Fones, H.N., Preston, G.M. & Smith, J.A.C. (2019) Variation in defence strategies in the metal hyperaccumulator plant *Noccaea caerulescens* is indicative of synergies and trade-offs between forms of defence. *Royal Society Open Science*, 6, 172418.
- Gradogna, A., Scholz-Starke, J., Gutla, P.V.K. & Carpaneto, A. (2009) Fluorescence combined with excised patch: measuring calcium currents in plant cation channels. *The Plant Journal*, 58, 175–182.
- Gradogna, A., Scholz-Starke, J., Pardo, J.M. & Carpaneto, A. (2021) Beyond the patch-clamp resolution: functional activity of non-electrogenic vacuolar NHX proton/potassium antiporters and inhibition by phosphoinositides. *New Phytologist*, 229, 3026–3036.
- Grynkiewicz, G., Poenie, M. & Tsien, R.Y. (1985) A new generation of Ca^{2+} indicators with greatly improved fluorescence properties. *Journal of Biological Chemistry*, 260, 3440–3450.
- Gulcicek, E.E., Colangelo, C.M., McMurray, W., Stone, K., Williams, K., Wu, T. et al. (2005). Proteomics and the analysis of proteomic data: an overview of current protein-profiling technologies. *Current Protocols in Bioinformatics*. <https://doi.org/10.1002/0471250953.bi1301s10>
- Hindt, M.N., Akmakjian, G.Z., Pivarski, K.L., Punshon, T., Baxter, I., Salt, D.E. et al. (2017) BRUTUS and its paralogs, BTS LIKE1 and BTS LIKE2, encode important negative regulators of the iron deficiency response in *Arabidopsis thaliana*. *Metallomics*, 9, 876–890.
- Hirschi, K.D. (2004) The calcium conundrum: both versatile nutrient and specific signal. *Plant Physiology*, 136, 2438–2442.
- Hirschi, K.D., Zhen, R.-G., Cunningham, K.W., Rea, P.A. & Fink, G.R. (1996) CAX1, an $\text{H}^{+}/\text{Ca}^{2+}$ antiporter from *Arabidopsis*. *Proceedings of the National Academy of Sciences*, 93, 8782–8786.
- Hocking, B., Conn, S.J., Manohar, M., Xu, B., Athman, A., Stancombe, M.A. et al. (2017) Heterodimerization of *Arabidopsis* calcium/proton exchangers contributes to regulation of guard cell dynamics and plant defense responses. *Journal of Experimental Botany*, 68, 4171–4183.
- Hogan, P.G. & Rao, A. (2015) Store-operated calcium entry: mechanisms and modulation. *Biochemical and Biophysical Research Communications*, 460, 40–49.
- Hu, S., Peng, L., Kwak, Y.-T., Tekippe, E.M., Pasare, C., Malter, J.S. et al. (2015) The DNA sensor AIM2 maintains intestinal homeostasis via regulation of epithelial antimicrobial host defense. *Cell Reports*, 13, 1922–1936.
- Huang, D. W., Sherman, B. T. & Lempicki, R. A. (2009). Bioinformatics enrichment tools: paths toward the comprehensive functional analysis of large gene lists. *Nucleic Acids Research*, 37(1), 1–13. <https://doi.org/10.1093/nar/gkn923>
- Liang, Y., Urano, D., Liao, K.L., Hedrick, T.L., Gao, Y. & Jones, A.M. (2017) A nondestructive method to estimate the chlorophyll content of *Arabidopsis* seedlings. *Plant Methods*, 13, 26.
- Liu, T.-Y., Aung, K., Tseng, C.-Y., Chang, T.-Y., Chen, Y.-S. & Chiou, T.-J. (2011) Vacuolar $\text{Ca}^{2+}/\text{H}^{+}$ transport activity is required for systemic phosphate homeostasis involving shoot-to-root signaling in *Arabidopsis*. *Plant Physiology*, 156, 1176–1189.
- Manohar, M., Shigaki, T. & Hirschi, K.D. (2011a) Plant cation/ H^{+} exchangers (CAXs): biological functions and genetic manipulations: plant cation/ H^{+} exchangers (CAXs). *Plant Biology*, 13, 561–569.
- Manohar, M., Shigaki, T., Mei, H., Park, S., Marshall, J., Aguilar, J. et al. (2011b) Characterization of *Arabidopsis* $\text{Ca}^{2+}/\text{H}^{+}$ exchanger CAX3. *Biochemistry*, 50, 6189–6195.
- Marty, F. (1999) Plant vacuoles. *The Plant Cell*, 11, 587–599.
- Modareszadeh, M., Bahmani, R., Kim, D. & Hwang, S. (2021) CAX3 (cation/proton exchanger) mediates a Cd tolerance by decreasing ROS through Ca elevation in *Arabidopsis*. *Plant Molecular Biology*, 105, 115–132.
- Noctor, G., Lelarge-Trouverie, C. & Mhamdi, A. (2015) The metabolomics of oxidative stress. *Phytochemistry*, 112, 33–53.
- Paradiso, A., Caretto, S., Leone, A., Bove, A., Nisi, R. & De Gara, L. (2016) ROS production and scavenging under anoxia and re-oxygenation in *Arabidopsis* cells: a balance between redox signaling and impairment. *Frontiers in Plant Science*, 7, 1803.
- Perteau, M., Perteau, G.M., Antonescu, C.M., Chang, T.C., Mendell, J.T. & Salzberg, S.L. (2015) StringTie enables improved reconstruction of a transcriptome from RNA-seq reads. *Nature Biotechnology*, 33, 290–295.
- Pittman, J.K. & Hirschi, K.D. (2016a) CAX-ing a wide net: cation/ H^{+} transporters in metal remediation and abiotic stress signalling. *Plant Biology*, 18, 741–749.
- Pittman, J.K. & Hirschi, K.D. (2016b) Phylogenetic analysis and protein structure modelling identifies distinct Ca^{2+} /Cation antiporters and conservation of gene family structure within *Arabidopsis* and rice species. *Rice*, 9, 1–6.
- Pittman, J.K., Shigaki, T. & Hirschi, K.D. (2005) Evidence of differential pH regulation of the *Arabidopsis* vacuolar $\text{Ca}^{2+}/\text{H}^{+}$ antiporters CAX1 and CAX2. *FEBS Letters*, 579, 2648–2656.
- Punshon, T., Hirschi, K., Yang, J., Lanzirrotti, A., Lai, B. & Guerinot, M.L. (2012) The role of CAX1 and CAX3 in elemental distribution and abundance in *Arabidopsis* seed. *Plant Physiology*, 158, 352–362.
- Ricachenevsky, F.K., Punshon, T., Salt, D.E., Fett, J.P. & Guerinot, M.L. (2021) *Arabidopsis thaliana* zinc accumulation in leaf trichomes is correlated with zinc concentration in leaves. *Scientific Reports*, 11, 5278.

- Sanders, D., Pelloux, J., Brownlee, C. & Harper, J.F. (2002) Calcium at the crossroads of signaling. *The Plant Cell*, 14, S401–S417.
- Searle, B.C. (2010) Scaffold: a bioinformatic tool for validating MS/MS-based proteomic studies. *Proteomics*, 10(6), 1265–1269. <https://doi.org/10.1002/pmic.200900437>
- Schachtman, D.P. & Shin, R. (2007) Nutrient sensing and signaling: NPKS. *Annual Review of Plant Biology*, 58, 47–69.
- Schönknecht, G. (2013) Calcium signals from the vacuole. *Plants*, 2, 589–614.
- Strazzer, P., Spelt, C.E., Li, S., Bliet, M., Federici, C.T., Roose, M.L. et al. (2019) Hyperacidification of *Citrus* fruits by a vacuolar proton-pumping P-ATPase complex. *Nature Communications*, 10, 744.
- Sze, H. & Chanroj, S. (2018) Plant endomembrane dynamics: studies of K(+)/H(+) antiporters provide insights on the effects of pH and ion homeostasis. *Plant Physiology*, 177, 875–895.
- Sze, H., Li, X., Palmgren, M.G., Sze, H., Li, X. & Palmgren, M.G. (1999) Energization of plant cell membranes by H⁺-pumping ATPases: regulation and biosynthesis. *The Plant Cell*, 11, 677–689.
- Sze, H., Liang, F., Hwang, I., Curran, A.C. & Harper, J.F. (2000) Diversity and regulation of plant Ca²⁺ pumps: insights from expression in yeast. *Annual Review of Plant Physiology and Plant Molecular Biology*, 51, 433–462.
- Whitt, L., Ricachenevsky, F.K., Ziegler, G.Z., Clemens, S., Walker, E., Maathuis, F.J.M. et al. (2020) A curated list of genes that affect the plant ionome. *Plant Direct*, 4, e00272.
- Xu, Y.C. & Guo, Y.L. (2020) Less is more, natural loss-of-function mutation is a strategy for adaptation. *Plant communication*, 1(6), 100103. <https://doi10.1016/j.xplc.2020.100103>
- Yang, J., Mathew, I.E., Rhein, H., Barker, R., Guo, Q., Brunello, L. et al. (2022) The vacuolar H⁺/Ca transporter CAX1 participates in submergence and anoxia stress responses. *Plant Physiology*, 190, 2617–2636.

SUPPORTING INFORMATION

Additional supporting information can be found online in the Supporting Information section at the end of this article.

How to cite this article: Mathew, I.E., Rhein, H.S., Yang, J., Gradogna, A., Carpaneto, A., Guo, Q. et al. (2024) Sequential removal of cation/H⁺ exchangers reveals their additive role in elemental distribution, calcium depletion and anoxia tolerance. *Plant, Cell & Environment*, 47, 557–573. <https://doi.org/10.1111/pce.14756>